Journal of Ultrafine Grained and Nanostructured Materials
https://jufgnsm.ut.ac.ir
Vol. 51, No.1, June 2018, pp. 32-42
Print ISSN: 2423-6845 Online ISSN: 2423-6837
DOI: 10.22059/JUFGNSM.2018.01.05

Synthesis and characterization of porous zinc oxide nano-flakes film in alkaline media

Arsalan Ravanbakhsh[1], Fereshteh Rashchi*[,1], Mahmoud Heydarzadeh Sohi[1], Rasoul Khayyam Nekouei[2], Mohammadreza Mortazavi Samarin[1]

[1]School of Metallurgy and Materials Engineering, College of Engineering, University of Tehran, Tehran, Iran.

[2]School of Materials Science & Engineering, University of New South Wales (UNSW), Sydney, NSW, Australia.

Recieved: 19 January 2018; Accepted: 19 March 2018

** Corresponding author email: rashchi@ut.ac.ir*

ABSTRACT

In this study, porous zinc oxide nano-flakes were successfully synthesized by anodization method on zinc substrate in a 0.025 M NaOH and 0.05 M NH_4Cl solution with the voltage of 10 V at room temperature. The field emission scanning electron microscopy's (FESEM) images show the structural evolution during 90 min of the anodization process. They also demonstrate the dependency of growth of ZnO flakes on the grains of the zinc substrate. Regarding FESEM images and possible chemical reactions taking place during the anodization process, a growth mechanism and sequences for the formation of ZnO have proposed. The Pourbaix diagram also confirmed this possible mechanism. The elemental and phase analysis conducted on films proved the formation of the ZnO after the anodization process. The cyclic voltammetry showed the oxidation of zinc into zinc oxide is related to the -1.28 V peak and the peak of zinc oxide reduction is situated at -1.48 V. The band gap of anodized zinc foil was calculated to be 3.24 eV. The photocatalytic activity of synthesized thin films also was studied and the ImageJ software analysis showed a strong correlation between the photocatalytic activity and the portion of porosity in the synthesized films.

Keywords: *Porous Oxide; Anodization; Electrochemical Synthesis; Photocatalytic Activity; Band Gap.*

1. Introduction

Zinc oxide (ZnO) with a direct wide band gap of 3.37 eV and a large excitation binding energy of 60 meV at room temperature is a well-known semiconducting material. It offers a wide range of properties that make this material a top candidate for the use in a number of applications such as optoelectronics [1], solar cells [2], light-emitting diodes (LEDs) [1], photocatalysts [3, 4], and sensors for various applications like cancer detection [5].

Zinc oxide has been considered as a good substitute for TiO_2 because of its optoelectronic, catalytic, and photochemical properties along with its considerably lower cost [6]. The oxidizing power of ZnO is strong enough to decompose many organic compounds [7]. This is due to its valance band position that produce photo-generated holes with oxidizing power. Thus, ZnO has the ability to decompose many dyes and pollutants [8-10] and often has higher efficiency than TiO_2 [6] owing to its high ability of generation, mobility, and separation of photo-excited electrons and holes [11]. However, the photo-instability of ZnO due to the photo-corrosion under radiation of UV and visible light and at extreme pH values is a major drawback for this compound which can significantly decrease

the photo-catalytic activity of ZnO [6,12].

Zinc oxide can be fabricated into several nanoscale forms like nanoparticles, thin films, and other micro/nanostructures [13-17]. Among them, thin films have the higher importance because of the numerous novel applications they can offer [18]. Different approaches such as physical/chemical vapor deposition [19], radio frequency sputtering [20], sol-gel [21], cathodic deposition [22], and anodization [23] have been used to fabricate nanostructured ZnO thin films. Solution based electrochemical synthesis, in particular, has attracted the most attention in the past decades because of their flexibility and cost-efficiency even for large scale and industrial fabrication [13, 24, 25].

Anodization process, as a facile method, has been widely used to produce uniform and highly adhesive oxide films with different structures or even wear/corrosion resistant films. This flexibility is only obtained by adjusting the process parameters which led to different structures and properties. This can be achieved even if many factors are identical except one or two which may just be slightly different. This remarkable flexibility led to introduction of facile methodology for fabrication of novel materials for a wide range of applications [5, 26-30]. Masuda and Fukuda [31] have reported on two-step anodization of aluminum which resulted in a porous alumina membrane. Since then, there has been an intensive research on aluminum anodization. Afterwards, the researchers attempted to use this method on other metals in the same way; such as, Ti [32]. However, the number of reports on zinc anodization is not very comprehensive. Moreover, with the large number of effective parameters in this technique, the demand for probing more into this field is undeniable.

In the recent years, there have been several investigations on ZnO structures and properties fabricated by anodization method. Basu et al. [33] studied the morphology and optical properties of fabricated ZnO thin films by anodic oxidation method in an oxalic acid media. They showed the correlation between the porosity of films and their photo-luminescence spectra variation. Yamaguchi et al. [25] investigated the relation of formed ZnO crystallite size and the photo-degradation of acetaldehyde gas. He et al. [15] synthesized different structures of ZnO in the mixture of hydrofluoric acid and methanol media. They have also studied the wettability of ZnO films under effect of electrical field. Gilani et al. [34] synthesized ZnO thin films in NaOH and oxalic acid electrolyte and studied their antibacterial activity. Huang et al. [35] used same NaOH medium and evaluated the water splitting ability of synthesized films. On the other hand, Ni et al. [36] demonstrated that in NaOH medium with the presence of NH_4F, zinc oxide forms in particles rather than films with high integrity demonstrating the amazing flexibility of anodization process for production of variety of materials. Among these studies, considering the numerous effective factors included in the anodization process like time, voltage, temperature, type of electrolyte and its concentration, a comprehensive study of microstructure and the photocatalytic behavior of ZnO thin films still is essential to be studied deeper. Especially, the effect of structure on photocatalytic degradation and the correlation between the porosity of film and their photocatalytic efficiency, which is certainly an important factor, should be more investigated.

In this study, we fabricated ZnO thin films using the facile and efficient anodization method in an alkaline NaOH media. Since, chlorine has been considered as an influential factor on electrochemical synthesis of ZnO [37], the NH_4Cl also was added to the electrolyte. This study especially focuses on the formation of ZnO nanostructure in the alkaline sodium hydroxide medium, the way this formation affects the photocatalytic activity of thin films, and the role of porosity of films on this characteristic in particular.

2. Experimental

2.1. Materials and preparation

All chemical reagents were commercially available and supplied by Merck Co. (Germany) with analytical grade and were used, as received, without further purification. The zinc ingot with 99.99 purity, produced by Khalessazan Industrial Group, was wire cut into rectangle slices with 2×4 cm dimensions and the thickness of 0.5 mm. The zinc foils then mechanically polished to remove surface roughness and then degreased in ethanol for about 10 min in an ultrasonic bath (VGT-1713QTD, Korea) and dried in the air. Afterwards, the electropolishing treatment was conducted on samples prior to the anodization process to insure the smooth and mirror-like surface of all the samples. The electropolishing process was carried out for 15 min on a magnetic stirrer (IKA RH Basic

2, Germany) for good mixing of the electrolyte which was the mixture of ethanol and phosphoric acid with the ratio of 7:3, at temperatures below 5 °C to prevent etching of the zinc in the acidic solution. The voltage used was kept constant at 10 V during the process and a stainless steel plate was used as the counter electrode. Then, samples were rinsed by deionized water and dried in air. In order to have similar conditions and identical current density, the samples were insulated by tape before the anodization process. Thus, each sample had the area of 3.5 cm^2 in contact with the electrolyte.

2.2. Anodization process

The anodization process took place in a basic electrolyte containing 0.025 M NaOH and 0.05 M NH_4Cl as a complexing agent. The power supplier (IPC-SL20PRC, Iran) established the voltage of 10 V during the anodization process. The cell contained two electrodes at the distance of 10 cm from each other, electropolished zinc as the working electrode and the graphite as the counter electrode. The process initiation was at 25 °C which was increased later by only 1 °C after 90 min of anodization. In the end, the samples were thoroughly rinsed with deionized water and dried in air.

2.3. Characterization

In order to study the morphology of synthesized films a field emission electron microscope (Σigma-VP, Germany) was used. The elemental and phase analysis were conducted by energy dispersive x-ray spectroscopy (Σigma-Oxford Instrument, Germany) and Grazing incidence X-ray diffraction (GIXD) (PANalytical X'Pert Pro MPD) methods. The grazing angle was set to 5 degrees. The current magnitude versus time has been monitored during the process as well as the cyclic voltammetry diagram in the same electrolyte. In addition, the optical band gap was calculated by the diffusion reflectance spectroscope (DRS) (Avantes-Avaspec-2048 TEC). Pore density was analyzed using the "ImageJ" software [38].

2.4. Photocatalytic activity measurements

The photocatalytic activity of synthesized thin films was measured by monitoring the degradation of methyl orange at room temperature under radiation of UV light. For this purpose a 1×1 cm^2 piece of film was placed into 10 mL of methyl orange solution with the concentration of 10 ppm. A 400 W Ultra-Violet lamp (Osram-Ultramed FDA400, Germany) was used for the process with the 25 mm of distance from the surface of the solution. The duration of the process was 120 min from the time that the lamp was turned on. Samples were taken from the solution during this time in 30 min intervals. Moreover, before the process began, the solution with the film sample in it was placed in the darkness for 60 min in order to reach adsorption equilibrium. The methyl orange concentration was measured during the photocatalytic test by UV-Vis spectroscope (Shimadzu-UV3100, Japan).

3. Results and Discussion

Figure 1 shows the formation of zinc oxide on the surface of the electropolished zinc foil during the anodization process. Figure 1-a demonstrates that the substrate was prepared properly and no considerable roughness could be seen on the surface after the electropolishing process even in the microscopic scale. The anodization process was conducted in 0.025 M sodium hydroxide and 0.05 M ammonium chloride aqueous solution using 10 V direct current. In the first stages of the anodization, it can be observed that small crevices are formed on the surface (Figure 1-b). With the continuation of the process, the depth of these crevices increased steadily and the ledges grew simultaneously to the point that new nuclei formed on the ledges (Figures 1-c and 1-d). The nuclei eventually grew and zinc oxide flakes formed homogeneously all over the surface (Figure 1-e). The research of Hu et al. [13] on zinc anodization in sodium bicarbonate solution confirms this results.

It can be inferred that dissolving of zinc ions into the solution and presence of OH^- in the solution as well as its production in the cathodic reaction plays the vital role in the formation of ZnO, as given in the following reactions [39].

$$O_2 + 2H_2O + 4e^- \leftrightarrow 4OH^- \quad \text{(at the cathode)} \quad \text{(eq. 1)}$$

$$NaOH \rightarrow Na^+ + OH^- \quad \text{(in the electrolyte)} \quad \text{(eq. 2)}$$

$$Zn \leftrightarrow Zn^{2+} + 2e^- \quad \text{(at the anode)} \quad \text{(eq. 3)}$$

$$Zn^{2+} + 2OH^- \rightarrow ZnO + H_2O \quad \text{(eq. 4)}$$

$$Zn^{2+} + \tfrac{1}{2}\, O_2 + 2e^- \leftrightarrow ZnO \quad \text{(overall reaction)} \quad \text{(eq. 5)}$$

This perfectly matches with the morphology variation during the process in Figure 1. Dissolving of zinc ions along with the formation of ZnO on the

substrate will eventually lead to the formation of crevices on the surface. Afterwards, as the process continues, these crevices grow in depth. Thus, the ledges has thinner electrical double layer and the OH^- ions are more likely to reach the ledges by diffusion through the double layer. Therefore, the nucleation and growth process occur more easily on the ledges than other parts (Figure 1-d). The 2D growth of zinc oxide depends on the properties of the substrate. Figure 2 shows the orientation of the zinc substrate's grains that control the growth of oxide flakes.

Figure 3 shows the Pourbaix diagrams of solutions containing 0.025 M NaOH, 0.05 M

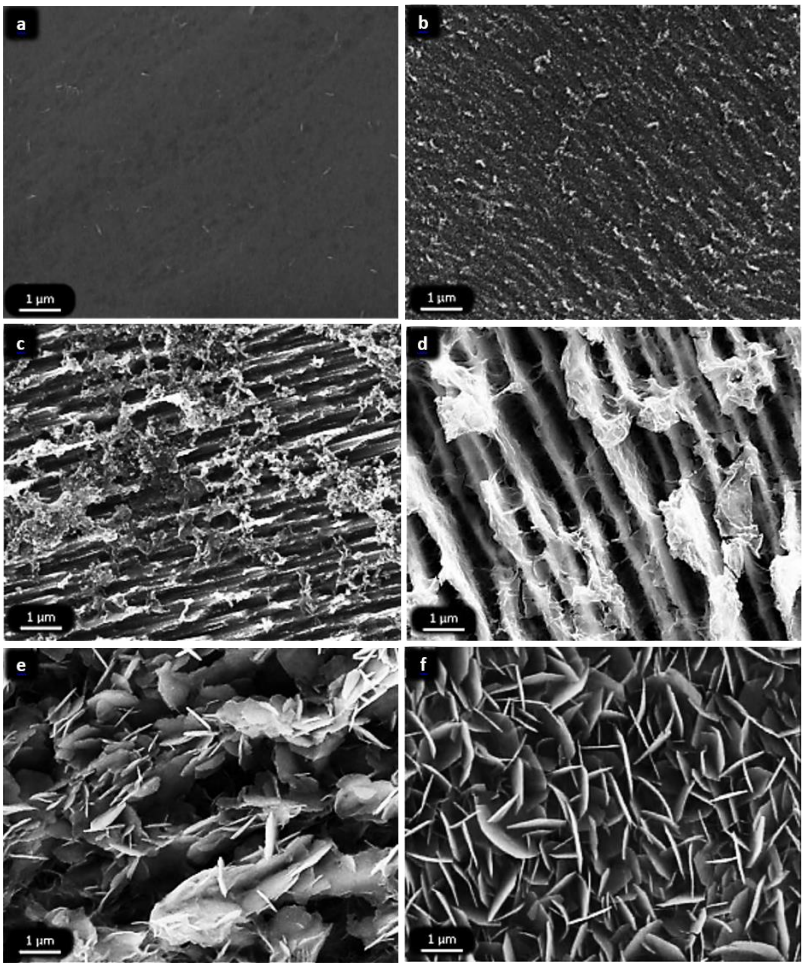

Fig. 1- Formation of zinc oxide during the anodization process on the surface of electropolished zinc substrate in a 0.025 M NaOH and 0.05 M NH_4Cl solution with the voltage of 10 V after (b) 5 min, (c) 15 min, (d) 30 min (e) 60 min, and (f) 90 min of the anodization process.

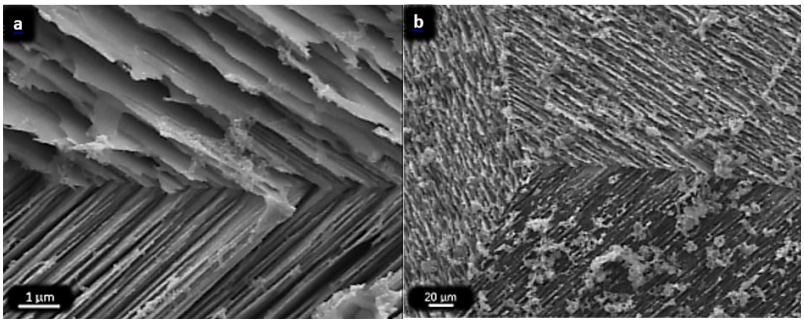

Fig. 2- ZnO nanoflakes orientation dependency on zinc substrate grains in different magnifications of (a) 3000X and (b) 300X.

NH_4Cl and different zinc concentrations. The figure shows that in the bulk solution, which has no initial zinc ions, the zinc hydroxide is the stable phase. However, in the vicinity of the anode, where the zinc ions enter the solution, higher zinc ion concentration leads to stability of ZnO phase.

Figure 4 shows the current density (I) vs. time (t) diagram for anodized sample in 0.025 M NaOH, 0.05 M NH_4Cl solution and 10 V potential. The current magnitude decreased severely in the initial period of the anodization process and as the process continued the rate of current reduction declined steadily. The formation of oxide layer on the surface is responsible for this current drop. In other words, in the beginning of the process the oxide layer forms rapidly and the thicker this layer becomes, the higher resistance it causes and it would enforce the current to drop. Eventually, the rate of oxide layer formation decreases.

The cyclic voltammetry of zinc foil in 0.025 M NaOH and 0.05 M NH_4Cl solution is shown in Figure 5. The oxidation of zinc into zinc oxide is related to the -1.28 V peak and the peak of zinc oxide reduction is situated at -1.48 V. These results are consistent with the results of other investigations on cyclic voltammetry of zinc [40, 41].

Phase and elemental analysis also were done on sample anodized in 0.025 M NaOH, 0.05 M NH_4Cl solution for 90 min and 10 V potential. The EDS analysis which is shown in Table 1 confirms the presence of Zn, O, and Cl on the surface of the sample. The chlorine ions may be remained from solution. As it can be seen from Table 1, as the process continues, the portion of Zn decreases, at the same time that of O increases. Thus, the ratio of O/Zn goes up. Although the portion of oxygen and zinc seems to be identical to form ZnO compound, the phase analysis was needed in

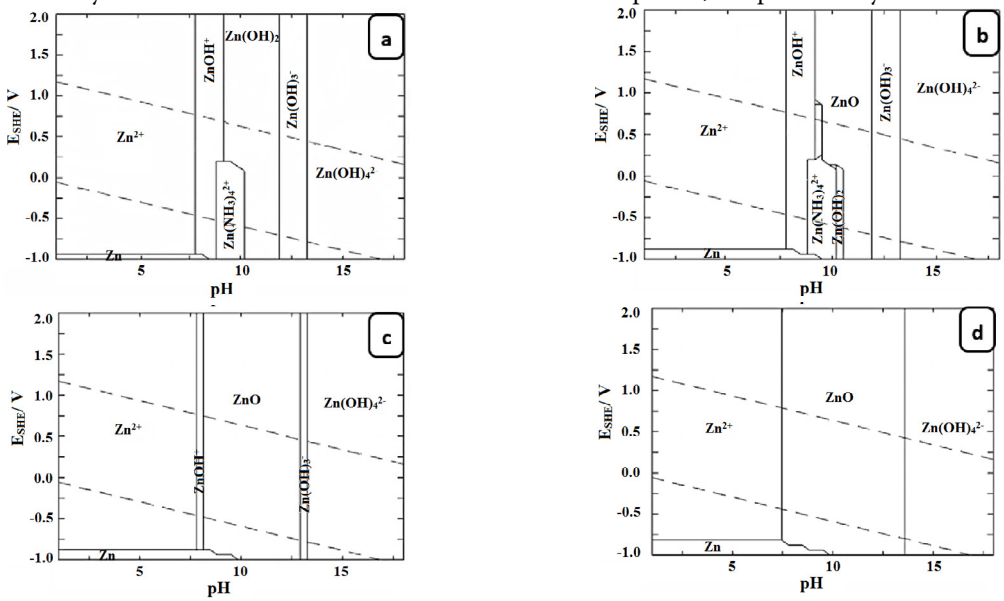

Fig. 3- Pourbaix diagram of 0.025 M NaOH and 0.05 M NH_4Cl containing (a) 0.1 µM, (b) 10 µM, (c) 100 µM and (d) 1000 µM zinc at room temperature.

Table 1- The EDS analysis of samples after different stages of the anodization process

Process Time (min)	Zn (at%)	O (at%)	Cl (at%)	O/Zn Ratio
5	78.65	23.13	1.78	0.29
15	67.12	35.44	2.56	0.53
30	61.29	41.79	3.08	0.68
60	57.34	46.27	3.61	0.81
90	55.69	48.16	3.85	0.86

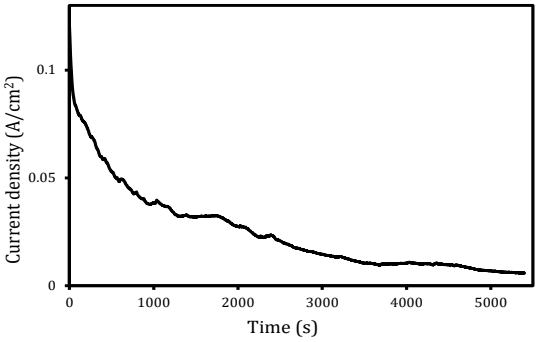

Fig. 4- The current density vs time plot of the anodization process in a 0.025 M NaOH and 0.05 M NH_4Cl and the voltage of 10 V.

order to assure the formation of ZnO. Hence, the GIXD pattern acquired which is shown in Figure 6. The pattern illustrates the presence of zinc oxide and zinc metal itself. It is apparent that zinc oxide layer is formed and the oxygen detected in the EDS analysis is in the form of ZnO compound as wurtzite. Since the GIXD pattern shows a complex set of peaks, we can conclude that the formed ZnO layer is polycrystalline [35, 42]. In addition, the zinc metal in the pattern was detected from the zinc foil substrate. The full width of half maximum (FWHM) of the diffraction peak can be used to calculate the crystallite size (D) of ZnO film by the Scherrer's formula:

$$D = 0.94\lambda/FWHM\ Cos\theta \quad \text{(eq. 6)}$$

The (0 0 2) peak was used to estimate the crystallite size, which was calculated to be 15 nm, that is in conformity with results of Ismail and Abdullah [42].

The optical properties of synthesized thin films were also studied by the DRS method. The reflectance spectra of anodized film in 0.025 M NaOH, 0.05 M NH_4Cl solution and 10 V voltage for 90 min is shown in Figure 7. The drop in reflectance around wavelength of 400 nm is related to optical transitions taking place in the band gap [43]. Therefore, in order to obtain the band gap, the

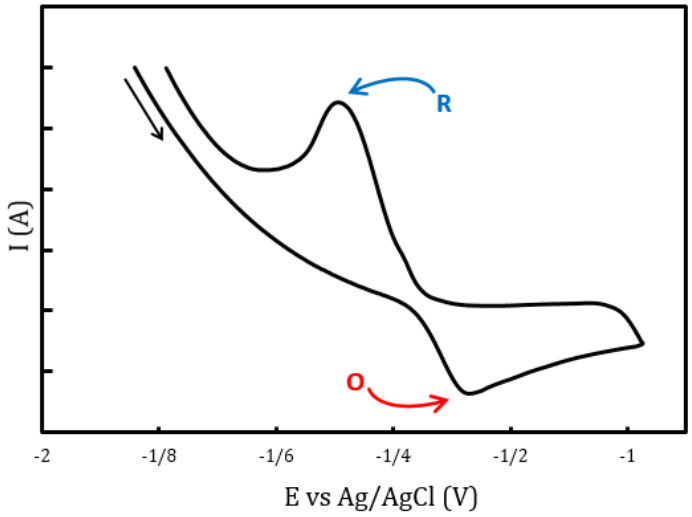

Fig. 5- The cyclic voltammetry of anodized zinc foil in a 0.025 M NaOH and 0.05 M NH_4Cl and the voltage of 10 V showing the oxidation (O) and the reduction (R) points of zinc and zinc oxide relatively.

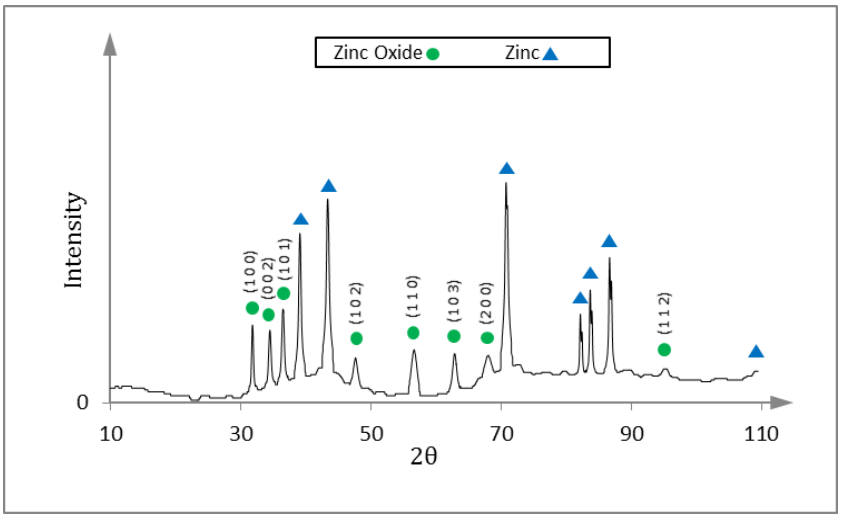

Fig. 6- The GIXD pattern of anodized zinc foil in a 0.025 M NaOH and 0.05 M NH_4Cl and the voltage of 10 V for 90 min.

reflectance spectra is transformed into absorbance spectra by the Kubleka-Munk [44] transformation which can be expressed as follows:

$$F(R) = \frac{(1-R)^2}{2R} = \frac{K}{S} \quad \text{(eq. 7)}$$

Where F(R) is the Kubelka-Munk function that is related to the amount of absorbance, R is the reflectance, K is the absorption coefficient, and S is the scattering coefficient. In semiconductors the optical transitions may be either direct or indirect. The equation for absorbance coefficient of direct semiconductors which zinc oxide is among them is [45]:

$$\alpha h\upsilon = A(h\upsilon - Eg)^n \quad \text{(eq. 8)}$$

where α is linear absorption coefficient of material, A is energy-independent constant, E_g is optical band gap, and n is a constant that indicates the type of optical transition, which is equal to 0.5 for direct transition [45]. In order to calculate F(R), equation (6) should be considered and since the Kubelka-Munk function is directly proportional to absorbance, F(R) values were converted into linear absorption coefficient through equation (8) as follows:

$$\alpha = \frac{F(R)}{t} = \frac{Absorbance}{t} \quad \text{(eq. 9)}$$

Where t is the film thickness which is assumed to be a unit in this study. Hence, by plotting $(\alpha h\nu)^2$ against hν and extrapolation, shown in Figure 8, the value of optical band gap of synthesized zinc oxide thin film was calculated to be 3.24 eV. This band gap value is in the range of reported band gap values for the zinc oxide [45]. However, the small difference between the calculated and theoretical

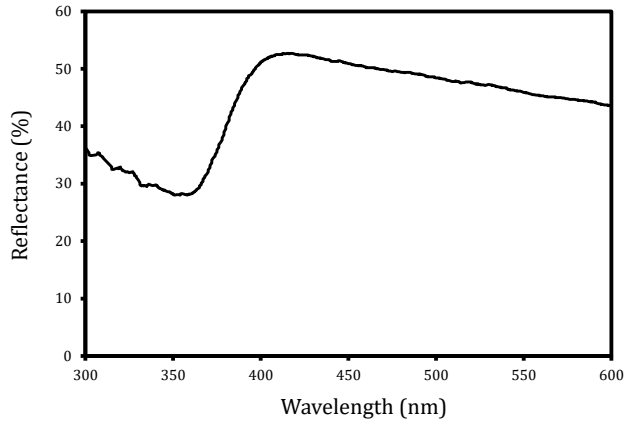

Fig. 7- The reflectance spectra of synthesized ZnO thin film.

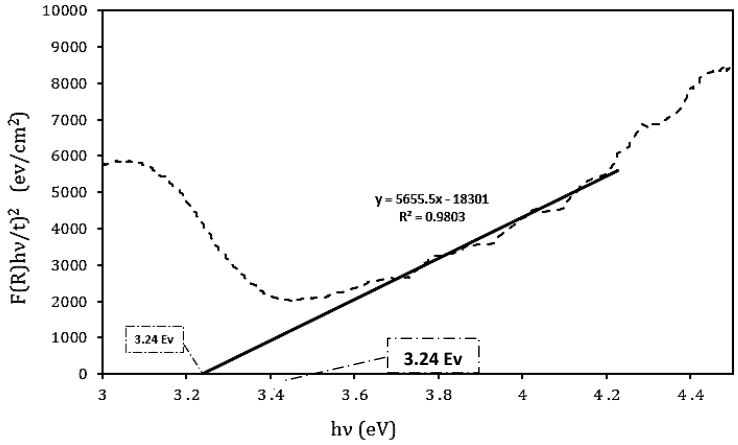

Fig. 8- The plot of $(\alpha h\nu)^2$ vs. hν for the anodized thin film.

band gap can be due to: 1) different synthesis approaches [43], 2) different microstructure and morphology of synthesized thin films which is related to absorption and scattering coefficient of the films [44], 3) Quantum confinement of the structure [46].

The photocatalytic behavior of anodized zinc foil has also been investigated in this study. Figure 9 illustrates the absorbance spectra of methylene orange (MO) in solution after 0, 30, 60, 90, and 120 minutes under radiation of UV light in the presence of synthesized thin film anodized in 0.025 M NaOH, 0.05 M NH_4Cl solution and 10 V voltage for 90 min. The ratio of peaks indicates the change in concentration of MO in the solution. Thus, the change in the concentration of MO during the photocatalysis test can be seen in Figure 10. It can be concluded from this diagram that the rate of MO degrading is relatively high during the first 30 minutes of the process. After this period, the rate decreased and then increased again. Since the oxygen plays a vital role in photocatalytic activity of semiconductors [47], the initial high rate of decomposition may be due to the presence of oxygen in the solution. As the MO decomposes, the oxygen content reduces to the extent that its concentration in the solution reaches a steady state. At this point the initial high rate of decomposition declines.

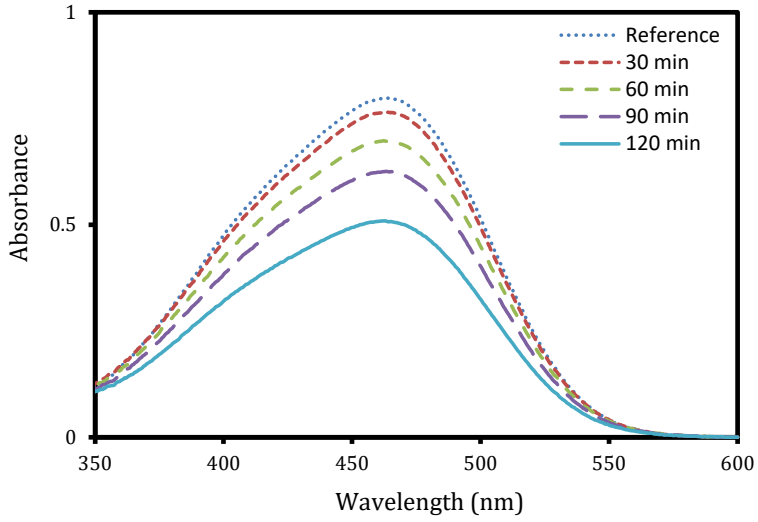

Fig. 9- UV-Vis absorbance spectra of methylene orange in different radiation intervals.

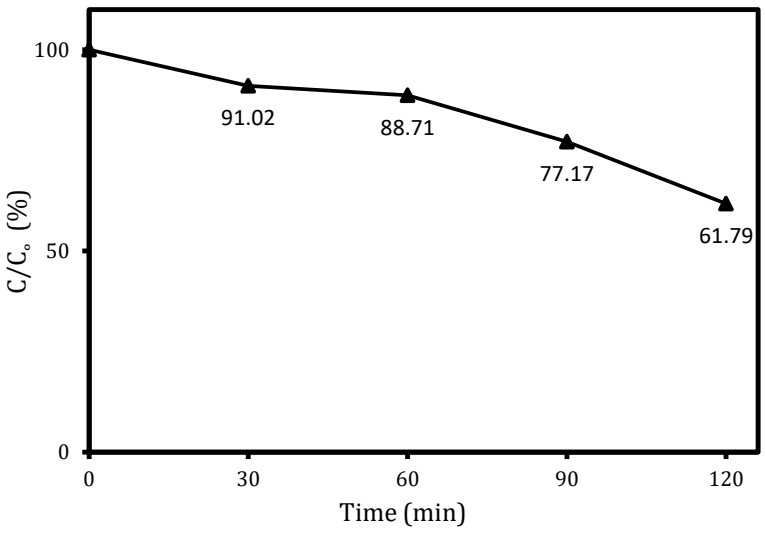

Fig. 10- Methylene orange concentration change during 120 min of UV light radiation for the sample anodized for 90 min.

Thus, if we neglect the first 30 min interval, it can be assumed that as the time passes the rate of MO degrading increases. In other words, there is a delay in the degrading of MO, after the moment radiation of UV light started. This behavior is identical for photocatalytic behavior of semiconductors without using an oxidizing agent in the solution [14].

The final percentage of MO degradation was specified as a measure for photocatalytic activity of samples. Thus, the amount of degradation of anodized samples after 120 min of UV light radiation is shown in Figure 11. The diagram shows that as the anodization time passes, larger portion of MO has decomposed during the photocatalytic activity. The interesting point is that during the initial stages of the anodization process photocatalytic activity of thin films increased dramatically; because even a small amount of oxide phase on the surface would enhance this quality significantly. After formation of the oxide phase, the extension of this growth would eventually lead to creation of a porous structure, as can be seen in Figure 1. The development of this porous layer does not only affect the absorption properties of thin films, but also it can expand the area of thin films which is in contact with the liquid. Both these factors made the escalating trend in degradation percentage after 15 min of anodization process in Figure 11.

Based on the analysis carried out by the ImageJ software which is shown in Figure 12, there is a strong correlation between the amount of porosity and the photocatalytic activity of synthesized films. It is clear that as the anodization process continues, the amount of porosity increases, as well as the photocatalytic activity. This is evident regarding Figures 11 and 12.

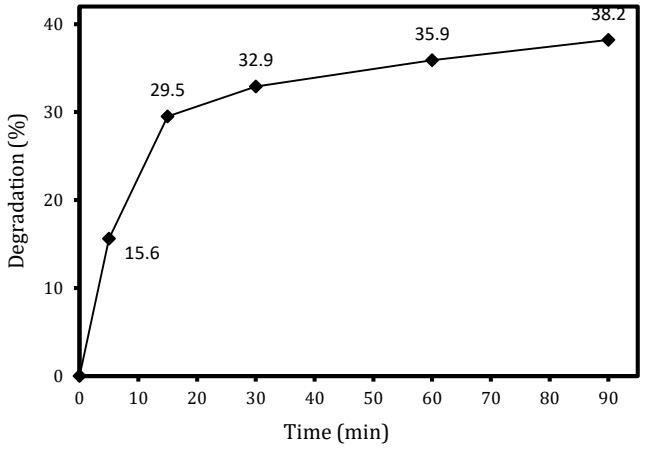

Fig. 11- Percentage of degradation by samples anodized for different periods of time.

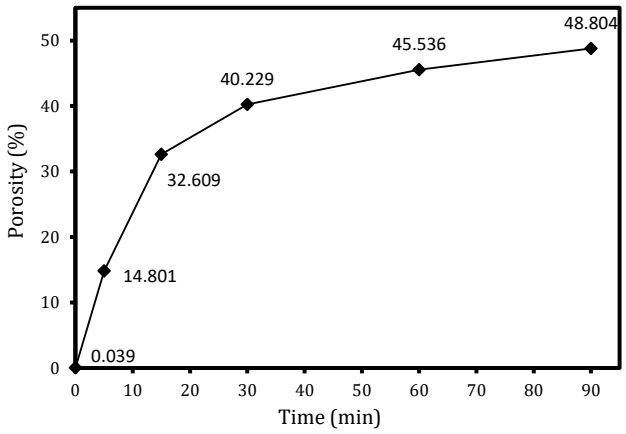

Fig. 12- The calculated porosity for samples anodized for different periods of time.

4. Conclusions

- Porous nano-flake zinc oxide thin film successfully synthesized in a 0.025 M NaOH and 0.05 M NH_4Cl solution with the voltage of 10 V at room temperature of 25 °C. The FESEM images show the structural evolution during 90 min of the anodization process. They also demonstrate the dependency of growth of ZnO flakes on the grains of the zinc substrate.
- The cyclic voltammetry show the oxidation of zinc into zinc oxide is related to the -1.28 V peak and the peak of zinc oxide reduction is situated at -1.48 V.
- A growth mechanism for formation of ZnO nanoflakes is proposed regarding FESEM images and possible chemical reactions during the anodization process in alkaline NaOH media. The mechanism is also confirmed by the calculated Pourbaix diagrams.
- The elemental (EDS) and phase analysis (GIXD) of synthesized films prove the formation of the ZnO after the anodization process.
- The bandgap of anodized zinc foil is calculated by the means of DRS and Kubleka-Munk transformation to be 3.24 eV.
- The photocatalytic activity of synthesized thin films also studied using methyl orange. During the initial stages of the anodization process photocatalytic activity of thin films increases dramatically. After formation of oxide phase, the extension of this growth would eventually lead to creation of a porous structure. The development of this porous layer does not only affect the absorption properties of thin films, but also it can expand the area of thin films which is in contact with the liquid.
- The ImageJ software analysis shows a strong correlation between the photocatalytic activity and the portion of porosity. As the anodization process goes on, the amount of porosity increases as well as the photocatalytic activity.

References

1. Look DC, Claflin B, Alivov YI, Park SJ. The future of ZnO light emitters. physica status solidi (a). 2004;201(10):2203-12.
2. Zhang Q, Dandeneau CS, Zhou X, Cao G. ZnO Nanostructures for Dye-Sensitized Solar Cells. Advanced Materials. 2009;21(41):4087-108.
3. Daneshvar N, Salari D, Khataee AR. Photocatalytic degradation of azo dye acid red 14 in water on ZnO as an alternative catalyst to TiO2. Journal of Photochemistry and Photobiology A: Chemistry. 2004;162(2-3):317-22.
4. Xiao F, Wang F, Fu X, Zheng Y. A green and facile self-assembly preparation of gold nanoparticles/ZnO nanocomposite for photocatalytic and photoelectrochemical applications. Journal of Materials Chemistry. 2012;22(7):2868.
5. Katwal G, Paulose M, Rusakova IA, Martinez JE, Varghese OK. Rapid Growth of Zinc Oxide Nanotube–Nanowire Hybrid Architectures and Their Use in Breast Cancer-Related Volatile Organics Detection. Nano Letters. 2016;16(5):3014-21.
6. Di Paola A, García-López E, Marcì G, Palmisano L. A survey of photocatalytic materials for environmental remediation. Journal of Hazardous Materials. 2012;211-212:3-29.
7. Miyauchi M, Nakajima A, Watanabe T, Hashimoto K. Photocatalysis and Photoinduced Hydrophilicity of Various Metal Oxide Thin Films. Chemistry of Materials. 2002;14(6):2812-6.
8. Kandavelu V, Kastien H, Thampi KR. Photocatalytic degradation of isothiazolin-3-ones in water and emulsion paints containing nanocrystalline TiO2 and ZnO catalysts. Applied Catalysis B: Environmental. 2004;48(2):101-11.
9. Abdel Aal A, Mahmoud SA, Aboul-Gheit AK. Sol–Gel and Thermally Evaporated Nanostructured Thin ZnO Films for Photocatalytic Degradation of Trichlorophenol. Nanoscale Research Letters. 2009;4(7):627-34.
10. Neppolian B, Sakthivel S, Arabindoo B, Palanichamy M, Murugesan V. Degradation of textile dye by solar light using TiO2and ZnO photocatalysts. Journal of Environmental Science and Health, Part A. 1999;34(9):1829-38.
11. Li Y, Xie W, Hu X, Shen G, Zhou X, Xiang Y, et al. Comparison of Dye Photodegradation and its Coupling with Light-to-Electricity Conversion over TiO2and ZnO. Langmuir. 2010;26(1):591-7.
12. de Jongh PE, Meulenkamp EA, Vanmaekelbergh D, Kelly JJ. Charge Carrier Dynamics in Illuminated, Particulate ZnO Electrodes. The Journal of Physical Chemistry B. 2000;104(32):7686-93.
13. Hu Z, Chen Q, Li Z, Yu Y, Peng L-M. Large-Scale and Rapid Synthesis of Ultralong ZnO Nanowire Films via Anodization. The Journal of Physical Chemistry C. 2009;114(2):881-9.
14. Moghaddam J, Mollaesmail S, Karimi S. The Influence of Morphology on Photo-catalytic Activity and Optical Properties of Nanocrystalline ZnO Powder. Nano-Micro Letters. 2012;4(4):197-201.
15. He S, Zheng M, Yao L, Yuan X, Li M, Ma L, et al. Preparation and properties of ZnO nanostructures by electrochemical anodization method. Applied Surface Science. 2010;256(8):2557-62.
16. Ye C, Bando Y, Shen G, Golberg D. Thickness-Dependent Photocatalytic Performance of ZnO Nanoplatelets. The Journal of Physical Chemistry B. 2006;110(31):15146-51.
17. Tian ZR, Voigt JA, Liu J, McKenzie B, McDermott MJ, Rodriguez MA, et al. Complex and oriented ZnO nanostructures. Nature Materials. 2003;2(12):821-6.
18. Peulon S. Mechanistic Study of Cathodic Electrodeposition of Zinc Oxide and Zinc Hydroxychloride Films from Oxygenated Aqueous Zinc Chloride Solutions. Journal of The Electrochemical Society. 1998;145(3):864.
19. Yang P, Yan H, Mao S, Russo R, Johnson J, Saykally R, et al. Controlled Growth of ZnO Nanowires and Their Optical Properties. Advanced Functional Materials. 2002;12(5):323.
20. Ellmer K, Wendt R. D.c. and r.f. (reactive) magnetron sputtering of ZnO:Al films from metallic and ceramic targets: a comparative study. Surface and Coatings Technology. 1997;93(1):21-6.
21. Kaneva N, Stambolova I, Blaskov V, Dimitriev Y, Vassilev S, Dushkin C. Photocatalytic activity of nanostructured ZnO films prepared by two different methods for the photoinitiated decolorization of malachite green. Journal of Alloys and Compounds. 2010;500(2):252-8.
22. Goux A, Pauporté T, Chivot J, Lincot D. Temperature effects on ZnO electrodeposition. Electrochimica Acta. 2005;50(11):2239-48.
23. Goh HS, Adnan R, Farrukh MA. ZnO nanoflake arrays prepared via anodization and their performance in the photodegradation of methyl orange. Turkish Journal of Chemistry. 2011 Jun 7;35(3):375-91.
24. Wang H-J, Sun Y-Y, Cao Y, Yu X-H, Ji X-M, Yang L.

Porous zinc oxide films: Controlled synthesis, cytotoxicity and photocatalytic activity. Chemical Engineering Journal. 2011;178:8-14.
25. Yamaguchi Y, Yamazaki M, Yoshihara S, Shirakashi T. Photocatalytic ZnO films prepared by anodizing. Journal of Electroanalytical Chemistry. 1998;442(1-2):1-3.
26. Voon CH, Lim BY, Hashim U, Md Arshad MK, Sam ST, Foo KL, et al. Effect of Temperature of Distilled Water on the Morphology of Nanoporous Zinc Oxide Synthesized by Anodizing. Applied Mechanics and Materials. 2015;754-755:1131-5.
27. Xiao F-X, Zeng Z, Liu B. Bridging the Gap: Electron Relay and Plasmonic Sensitization of Metal Nanocrystals for Metal Clusters. Journal of the American Chemical Society. 2015;137(33):10735-44.
28. Xiao F. Self-assembly preparation of gold nanoparticles-TiO2 nanotube arrays binary hybrid nanocomposites for photocatalytic applications. Journal of Materials Chemistry. 2012;22(16):7819.
29. Xiao F. An efficient layer-by-layer self-assembly of metal-TiO2 nanoring/nanotube heterostructures, M/T-NRNT (M = Au, Ag, Pt), for versatile catalytic applications. Chemical Communications. 2012;48(52):6538.
30. Xiao F. Layer-by-Layer Self-Assembly Construction of Highly Ordered Metal-TiO2 Nanotube Arrays Heterostructures (M/TNTs, M = Au, Ag, Pt) with Tunable Catalytic Activities. The Journal of Physical Chemistry C. 2012;116(31):16487-98.
31. Masuda H, Fukuda K. Ordered Metal Nanohole Arrays Made by a Two-Step Replication of Honeycomb Structures of Anodic Alumina. Science. 1995;268(5216):1466-8.
32. Liu R, Yang W-D, Qiang L-S, Wu J-F. Fabrication of TiO2 nanotube arrays by electrochemical anodization in an NH4F/H3PO4 electrolyte. Thin Solid Films. 2011;519(19):6459-66.
33. Basu PK, Saha N, Maji S, Saha H, Basu S. Nanoporous ZnO thin films deposited by electrochemical anodization: effect of UV light. Journal of Materials Science: Materials in Electronics. 2008;19(6):493-9.
34. Gilani S, Ghorbanpour M, Parchehbaf Jadid A. Antibacterial activity of ZnO films prepared by anodizing. Journal of Nanostructure in Chemistry. 2016;6(2):183-9.
35. Huang M-C, Wang T, Wu B-J, Lin J-C, Wu C-C. Anodized ZnO nanostructures for photoelectrochemical water splitting. Applied Surface Science. 2016;360:442-50.
36. Ni G, Chen Y, Liu Y, Liu H, Zhang Z. Fabrication of ZnO Nanoparticles for Photocatalytic Reduction of CO2. MATEC Web of Conferences. 2016;67:02009.
37. Lupan O, Pauporté T, Chow L, Viana B, Pellé F, Ono LK, et al. Effects of annealing on properties of ZnO thin films prepared by electrochemical deposition in chloride medium. Applied Surface Science. 2010;256(6):1895-907.
38. National Institutes of Health (NIH), ImageJ: Image Processing and Analysis Java software (Version 1.51). Available from https://imagej.nih.gov/ij/index.html
39. Toward Functional Nanomaterials. Springer US; 2009.
40. Jagadish C, Pearton SJ, editors. Zinc oxide bulk, thin films and nanostructures: processing, properties, and applications. Elsevier; 2011 Oct 10.
41. Look DC, Claflin B, Alivov YI, Park SJ. The future of ZnO light emitters. physica status solidi (a). 2004;201(10):2203-12.
42. Ismail A, Abdullah MJ. The structural and optical properties of ZnO thin films prepared at different RF sputtering power. Journal of King Saud University - Science. 2013;25(3):209-15.
43. Patil GE, Kajale DD, Gaikwad VB, Jain GH. Preparation and characterization of SnO2 nanoparticles by hydrothermal route. International Nano Letters. 2012;2(1).
44. Murphy A. Band-gap determination from diffuse reflectance measurements of semiconductor films, and application to photoelectrochemical water-splitting. Solar Energy Materials and Solar Cells. 2007;91(14):1326-37.
45. Morales AE, Mora ES, Pal U. Use of diffuse reflectance spectroscopy for optical characterization of un-supported nanostructures. Revista mexicana de física. 2007;53(5):18-22.
46. Zhu H, Yang D, Yu G, Zhang H, Yao K. A simple hydrothermal route for synthesizing SnO2 quantum dots. Nanotechnology. 2006;17(9):2386-9.
47. Hoffmann MR, Martin ST, Choi W, Bahnemann DW. Environmental Applications of Semiconductor Photocatalysis. Chemical Reviews. 1995;95(1):69-96.